(American Geophysical Union, Washington, DC, 1998), pp. 97–118.
7. M. Murakami, K. Hirose, K. Kawamura, N. Sata, Y. Ohishi, *Science* **304**, 855 (2004).
8. A. R. Oganov, S. Ono, *Nature* **430**, 445 (2004).
9. D. Helmberger, T. Lay, S. Ni, M. Gurnis, *Proc. Nat. Acad. Sci. U.S.A.* **102**, 17257 (2005).
10. J. Wookey, S. Stackhouse, J. Kendall, J. Brodholt, G. D. Price, *Nature* **438**, 1004 (2005).
11. K. Hirose, *Rev. Geophys.* **44**, RG3001 (2006).
12. W. L. Mao *et al.*, *Science* **312**, 564 (2006).
13. T. Lay, J. Hernlund, E. J. Garnero, M. S. Thorne, *Science* **314**, 1272 (2006).
14. Materials and methods are available as supporting material on *Science* Online.
15. J. Santillán, S. Shim, G. Shen, V. Prakapenka, *Geophys. Res. Lett.* **33**, L15307 (2006).
16. D. Yamazaki, T. Yoshino, H. Ohfuji, J. Ando, A. Yoneda, *Earth Planet. Sci. Lett.* **252**, 372 (2006).
17. S. Merkel *et al.*, *Science* **311**, 644 (2006).
18. R. A. Lebensohn, C. N. Tomé, *Acta Metal. Mater.* **41**, 2611 (1993).
19. A. R. Oganov, R. Martonák, A. Laio, P. Raiteri, M. Parrinello, *Nature* **438**, 1142 (2005).
20. P. Carrez, D. Ferré, P. Cordier, *Nature* **446**, 68 (2007).
21. L. Moresi, M. Gurnis, *Earth Planet. Sci. Lett.* **138**, 15 (1996).
22. A. K. McNamara, P. E. van Keken, S.-I. Karato, *J. Geophys. Res.* **108**, 2230 (2003).
23. A. K. McNamara, S. Zhong, *Earth Planet. Sci. Lett.* **222**, 485 (2004).
24. S. Stackhouse, J. P. Brodholt, J. Wookey, J.-M. Kendall, G. D. Price, *Earth Planet. Sci. Lett.* **230**, 1 (2005).
25. R. Wentzcovitch, T. Tsuchiya, J. Tsuchiya, *Proc. Nat. Acad. Sci. U.S.A.* **103**, 543 (2006).
26. M. Moore, E. J. Garnero, T. Lay, Q. Williams, *J. Geophys. Res.* **109**, B02319 (2004).
27. E. J. Garnero, V. Maupin, T. Lay, M. J. Fouch, *Science* **306**, 259 (2004).
28. J. Wookey, J. M. Kendall, G. Rümpker, *Geophys. J. Int.* **161**, 829 (2005).
29. S. A. Russell, T. Lay, E. J. Garnero, *Nature* **396**, 255 (1998).
30. S. A. Russell, T. Lay, E. J. Garnero, *J. Geophys. Res.* **104**, 13,183 (1999).
31. J. M. Rokosky, T. Lay, E. J. Garnero, *Earth Planet. Sci. Lett.* **248**, 411 (2006).

32. We thank D. Mainprice for his petrophysics software package, P. Liermann for assistance during the experiment, and the two anonymous reviewers for their comments. This work was supported by NSF grants EAR-0510383 and EAR-0456356 (T.S.D., H.R.W., and A.K.M.) and the Carnegie/Department of Energy Alliance Center (T.S.D. and H.R.W.). Experiments were performed at HPCAT (Sector 16), Advanced Photon Source (APS), Argonne National Laboratory. Use of the HPCAT facility was supported by Department of Energy (DOE) Basic Energy Sciences (BES), DOE National Nuclear Security Administration, NSF, Department of Defense (DOD) Tank-Automotive and Armaments Command, and the W. M. Keck Foundation. Use of the APS was supported by DOE-BES under contract W-31-109-ENG-38. S.M. and S.S. also acknowledge support from the Miller Institute for Basic Research in Science.

Supporting Online Material

www.sciencemag.org/cgi/content/full/316/5832/1729/DC1
Materials and Methods
Figs. S1 to S10
Tables S1 to S3
References

31 January 2007; accepted 13 April 2007
10.1126/science.1140609

Weak Northern and Strong Tropical Land Carbon Uptake from Vertical Profiles of Atmospheric CO_2

Britton B. Stephens,[1]* Kevin R. Gurney,[2] Pieter P. Tans,[3] Colm Sweeney,[3] Wouter Peters,[3] Lori Bruhwiler,[3] Philippe Ciais,[4] Michel Ramonet,[4] Philippe Bousquet,[4] Takakiyo Nakazawa,[5] Shuji Aoki,[5] Toshinobu Machida,[6] Gen Inoue,[7] Nikolay Vinnichenko,[8]† Jon Lloyd,[9] Armin Jordan,[10] Martin Heimann,[10] Olga Shibistova,[11] Ray L. Langenfelds,[12] L. Paul Steele,[12] Roger J. Francey,[12] A. Scott Denning[13]

Measurements of midday vertical atmospheric CO_2 distributions reveal annual-mean vertical CO_2 gradients that are inconsistent with atmospheric models that estimate a large transfer of terrestrial carbon from tropical to northern latitudes. The three models that most closely reproduce the observed annual-mean vertical CO_2 gradients estimate weaker northern uptake of −1.5 petagrams of carbon per year (Pg C year^{-1}) and weaker tropical emission of +0.1 Pg C year^{-1} compared with previous consensus estimates of −2.4 and +1.8 Pg C year^{-1}, respectively. This suggests that northern terrestrial uptake of industrial CO_2 emissions plays a smaller role than previously thought and that, after subtracting land-use emissions, tropical ecosystems may currently be strong sinks for CO_2.

Our ability to diagnose the fate of anthropogenic carbon emissions depends critically on interpreting spatial and temporal gradients of atmospheric CO_2 concentrations (*1*). Studies using global atmospheric transport models to infer surface fluxes from boundary-layer CO_2 concentration observations have generally estimated the northern mid-latitudes to be a sink of approximately 2 to 3.5 Pg C year^{-1} (*2*–*5*). Analyses of surface ocean partial pressure of CO_2 (*2*), atmospheric carbon isotope (*6*), and atmospheric oxygen (*7*) measurements have further indicated that most of this northern sink must reside on land. Tropical fluxes are not well constrained by the atmospheric observing network, but global mass-balance requirements have led to estimates of strong (1 to 2 Pg C year^{-1}) tropical carbon sources (*4*, *5*). Attribution of the Northern Hemisphere terrestrial carbon sink (*8*–*13*) and reconciliation of estimates of land-use carbon emissions and intact forest carbon uptake in the tropics (*14*–*19*) have motivated considerable research, but these fluxes remain quantitatively uncertain. The full range of results in a recent inverse model comparison study (*5*), and in independent studies (*3*, *20*, *21*), spans budgets with northern terrestrial uptake of 0.5 to 4 Pg C year^{-1}, and tropical terrestrial emissions of −1 to +4 Pg C year^{-1}. Here, we analyzed observations of the vertical distribution of CO_2 in the atmosphere that provide new constraints on the latitudinal distribution of carbon fluxes.

Previous inverse studies have used boundary-layer data almost exclusively. Flask samples from profiling aircraft have been collected and measured at a number of locations for up to several decades (*22*–*24*), but efforts to compile these observations from multiple institutions and to compare them with predictions of global models have been limited. Figure 1 shows average vertical profiles of atmospheric CO_2 derived from flask samples collected from aircraft during midday at 12 global locations (fig. S1), with records extending over periods from 4 to 27 years (table S1 and fig. S2) (*25*). These seasonal and annual-mean profiles reflect the combined influences of surface fluxes and atmospheric mixing. During the summer in the Northern Hemisphere, midday atmospheric CO_2 concentrations are generally lower near the surface than in the free troposphere, reflecting the greater impact of terrestrial photosynthesis over industrial emissions at this time. Sampling locations over or immediately downwind of continents show larger gradients than those over or downwind of ocean basins in response to stronger land-based fluxes, and higher-latitude locations show greater CO_2 drawdown at high altitude. Conversely, during the winter, respiration and fossil-fuel sources lead to elevated low-altitude atmospheric CO_2 concentrations at northern locations. The gradients are comparable in magnitude in both seasons, but the positive

[1]National Center for Atmospheric Research, Boulder, CO 80305, USA. [2]Department of Earth and Atmospheric Sciences, Purdue University, West Lafayette, IN 47907, USA. [3]National Oceanic and Atmospheric Administration, Boulder, CO 80305, USA. [4]Le Laboratoire des Sciences du Climat et l'Environnement, 91191 Gif sur Yvette, France. [5]Center for Atmospheric and Oceanic Studies, Tohoku University, Sendai 980-8578, Japan. [6]National Institute for Environmental Studies, Onogawa, Tsukuba 305-8506, Japan. [7]Graduate School of Environmental Studies, Nagoya University, Nagoya City 464-8601, Japan. [8]Central Aerological Observatory, Dolgoprudny, 141700, Russia. [9]School of Geography, University of Leeds, West Yorkshire, LS2 9JT, UK. [10]Max Planck Institute for Biogeochemistry, 07701 Jena, Germany. [11]Sukachev Institute of Forest, Krasnoyarsk, 660036, Russia. [12]Commonwealth Scientific and Industrial Research Organisation (CSIRO) Marine and Atmospheric Research, Aspendale, Victoria 3195, Australia. [13]Department of Atmospheric Science, Colorado State University, Fort Collins, CO 80523, USA.

*To whom correspondence should be addressed. E-mail: stephens@ucar.edu
†Deceased.

gradients persist for a greater portion of the year and the annual-mean gradients also show higher atmospheric CO_2 concentrations near the surface than aloft. We estimated average Northern Hemisphere profiles (thick black lines in Fig. 1) by combining records from 10 sites (*25*). We found average Northern Hemisphere midday differences between altitudes of 1 and 4 km of –2.2 parts per million (ppm) in summer, +2.6 ppm in winter, and +0.7 ppm in annual mean. The two Southern Hemisphere locations show relatively constant CO_2 profiles in all seasons, with slightly higher values in the free troposphere.

To assess the performance of global atmospheric transport models used in CO_2 inverse studies, we compared the model predictions to our observations. We sampled the post-inversion concentration fields from the 12 models participating in the Transcom 3 Level 2 seasonal inversion experiment (T3L2) (*5*) at the airborne sampling locations in Fig. 1 and then fit and averaged these model predictions in the same manner as the observations (*25*). The models reproduce the general features of depleted low-altitude CO_2 during the summer and enhanced low-altitude CO_2 during the winter, but with important systematic differences (Fig. 2). Most of the models have gradients that are too small in the summer (Fig. 2A), suggesting that these models ventilate too much of the CO_2 uptake signal at this time of year. In the winter, the models match the observed gradients on average but include cases where vertical mixing appears both underestimated and overestimated. The predicted Northern Hemisphere annual-mean midday gradients are considerably larger than observed (Fig. 2B) and represent a substantial bias in the models. This overprediction of the annual-mean vertical gradients is also apparent when comparing models and data at individual sampling locations and is most pronounced at sites over or downwind of continents (fig. S6). The offset between the mean of the models and the observations at high-altitude in the summer (Fig. 2A) appears to be related to lags in the timing of the hemispheric CO_2 drawdown and to the fact that the models were optimized to marine boundary-layer stations, whereas the profile sites include measurements over the continental interiors. We focused only on the vertical gradients, which respond more quickly than the column means and are largely independent of where the models were optimized.

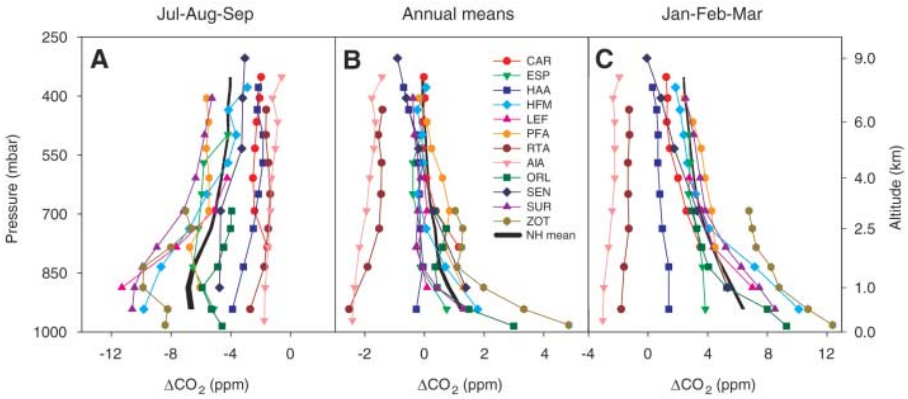

Fig. 1. Midday vertical CO_2 profiles measured at 12 global locations based on fits to samples binned by altitude and averaged over different seasonal intervals. Northern Hemisphere sites include Briggsdale, Colorado, United States (CAR); Estevan Point, British Columbia, Canada (ESP); Molokai Island, Hawaii, United States (HAA); Harvard Forest, Massachusetts, United States (HFM); Park Falls, Wisconsin, United States (LEF); Poker Flat, Alaska, United States (PFA); Orleans, France (ORL); Sendai/Fukuoka, Japan (SEN); Surgut, Russia (SUR); and Zotino, Russia (ZOT). Southern Hemisphere sites include Rarotonga, Cook Islands (RTA) and Bass Strait/Cape Grim, Australia (AIA). Profiles are averaged over Northern Hemisphere summer (**A**), all months (**B**), and Northern Hemisphere winter (**C**). A smoothed deseasonalized record from Mauna Loa has been subtracted from the observations at each site. Black lines in each panel represent Northern Hemisphere average profiles (center) and uncertainties (width) for the same times (*25*). The horizontal axis in (B) is zoomed by a factor of 2 relative to those in (A) and (C).

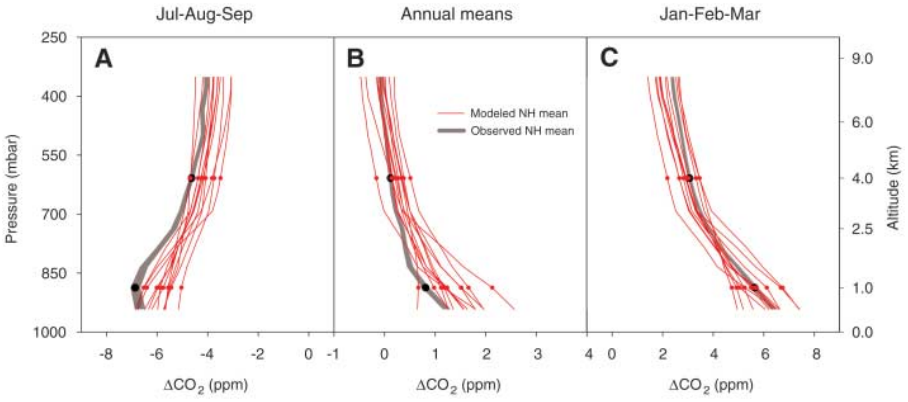

Fig. 2. (**A** to **C**) Observed Northern Hemisphere average profiles compared with predictions of the 12 T3L2 models over the same seasonal intervals as in Fig. 1. Gray lines indicate the observed average vertical CO_2 gradients (center) and uncertainties (width) from Fig. 1 (*25*). The model output was processed in the same way as the observations at each site before averaging (*25*). Symbols indicate 1- and 4-km values used for calculating the vertical gradients shown in Fig. 3. The horizontal axis in (B) is zoomed by a factor of 2 relative to those in (A) and (C).

Because the T3L2 models were primarily constrained by boundary-layer measurements, these post-inversion vertical gradients reflect the vertical mixing characteristics of the models [supporting online material (SOM) text]. Atmospheric mixing, surface CO_2 fluxes, and CO_2 spatial gradients are tightly linked in inverse calculations such that any biases in mixing, horizontal or vertical, will translate into biases in estimated fluxes. Figure 3 shows the impact of the range of vertical mixing behavior on northern and tropical land fluxes estimated using these models. Models that trap more CO_2 near the surface in the Northern Hemisphere during the winter require relatively weaker northern land emissions during this period to match surface observations, with a high degree of correlation (Fig. 3C). This vertical gradient-flux correlation is not as clear in the summer, probably because fossil-fuel burning and photosynthesis have opposing effects on concentration gradients, although there is a suggestion that models that ventilate summer uptake signals more efficiently require stronger northern land uptake to match the boundary-layer observations. These relationships are preserved when averaging over the annual cycle, and models with seasonal mixing characteristics that result in higher annually averaged CO_2 near the surface relative to aloft in the Northern Hemisphere estimate substantially greater annual-mean northern land uptake.

Because global CO_2 mass-balance must be maintained, and because the seasonally varying interaction of atmospheric mixing and terrestrial fluxes produces gradients primarily between northern and tropical latitudes, the models estimate compensating variations in tropical land fluxes in all three cases (Fig. 3). Models that estimate strong northern land uptake also estimate strong tropical land emissions. The tropical variations are larger and their correlations to the vertical gradients better than for the northern land fluxes, possibly because tropical fluxes are

less constrained by atmospheric CO_2 measurements and are consequently more susceptible to influence from model transport biases. These large across-model variations in northern and tropical land fluxes are not random, but are systematically related to how the models distribute CO_2 fluxes vertically in the Northern Hemisphere in different seasons.

The gray bars in Fig. 3 indicate the corresponding observed mean 1- to 4-km gradients and uncertainties (*25*) and reveal that most models overpredict the annual-mean midday vertical gradients. We considered a number of potential biases in comparing aircraft flask sample CO_2 measurements to model output. These include potential model biases related to diurnal flux variations and coarse grid resolution, and potential observation biases related to diurnal concentration variations, measurement representativeness, interannual variations, fair-weather flying conditions, and interlaboratory offsets (SOM text, tables S4 and S5, and figs. S8 and S9). Although the fair-weather bias can be as large as 1 ppm at individual sites, when averaging across the Northern Hemisphere, all of these potential biases appear to be smaller than 0.2 ppm or in the wrong direction to explain the model-observation differences shown in Figs. 2 and 3.

These differences suggest that an average taken across all models does not provide the most robust estimate of northern versus tropical flux partitioning. Furthermore, no single model captures both the seasonal and annual-mean observed gradients accurately (table S3). Because small seasonal flux errors of the same sign can combine to result in larger annual-mean flux biases, we used only annual-mean gradients to evaluate the models' annual-mean flux estimates. The three models closest to the annual-mean vertical gradients (models 4, 5, and C; tables S2 and S3) estimate average northern land uptake and tropical land emission of –1.5 ± 0.6 (±SD) and +0.1 ± 0.8 Pg C $year^{-1}$, respectively. The T3L2 12-model average northern and tropical land results were considerably different at –2.4 ± 1.1 and +1.8 ± 1.7 Pg C $year^{-1}$, respectively (*5*). Models 4, 5, and C have concentration biases in summer and winter that are substantial, but these errors offset rather than compound as they do for other models (table S3), which results in more accurate annual-mean gradients and consequently implies more accurate annual-mean flux estimates (SOM text).

Our results suggest less carbon uptake by northern land ecosystems than previously thought. Furthermore, because land-use changes in the tropics are thought to cause strong carbon emissions (*16*–*18*), our results imply strong carbon uptake in undisturbed ecosystems. These flux revisions are consistent with other lines of evidence and may help to resolve several long-standing conflicts in global carbon budgeting (*26*). Terrestrial ecosystem models and inventory studies have estimated northern terrestrial carbon uptake rates that are considerably weaker than suggested by the T3L2 study and other inverse models (*8*, *10*, *17*, *27*, *28*). In the tropics, theoretical reasons to expect strong carbon uptake fluxes in intact tropical forests (*29*) have been at odds with the strong emissions estimated in the T3L2 study. Tropical land carbon budgets are uncertain because of high spatial and interannual variability and a lack of comprehensive measurements (*30*, *31*), but a weak emission flux resulting from a relatively weaker deforestation source combined with a relatively stronger sink has support from bottom-up estimates (*14*–*16*, *18*, *19*, *32*). Notably, a repartitioning of terrestrial fluxes between northern and tropical regions as implied here does not conflict with independent ^{13}C and O_2/N_2 constraints on the global land-ocean flux partitioning.

A number of studies have stressed that because of the large differences seen between atmospheric inverse models, their estimated spatial distribution of annual-mean fluxes should be interpreted with great caution (*3*, *20*, *33*). Our analysis of the vertical distribution of atmospheric CO_2 suggests that these differences are systematic and open to validation. Other model properties, such as horizontal mixing aloft and seasonal timing of prior flux estimates, will have different effects on estimated fluxes and should also be investigated. The present airborne observing network is relatively sparse, and as more data become available our results may be refined. Also, we did not use interstation concentration differences in our analyses, but if interlaboratory calibration offsets are minimized, additional model tests may be possible. Future atmospheric inverse models with accurate seasonal mixing behavior will result in improved estimates of global carbon cycling. The continuation and expansion of airborne measurement programs for CO_2 and related tracers, and advances in coupled ecosystem-atmosphere modeling, including validation against discrete measurements, will greatly advance this goal.

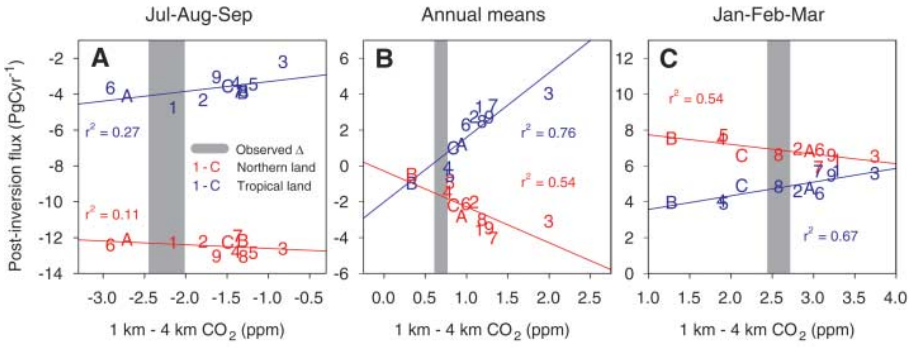

Fig. 3. Northern land and tropical land carbon fluxes for the 1992 to 1996 time period estimated by the 12 T3L2 models plotted as a function of the models' post-inversion predicted mean vertical CO_2 gradients for the same seasonal intervals as Fig. 1. The vertical axis in each plot represents the estimated fluxes for all northern land regions (red) and all tropical-land regions (blue) averaged over Northern Hemisphere summer (**A**), all months (**B**), and Northern Hemisphere winter (**C**). The horizontal axis represents the predicted Northern Hemisphere vertical CO_2 difference between 1- and 4-km altitude at these same times. The plotted numbers (1 to 9) and letters (A to C) correspond to the 12 models listed in table S2. Gray bars indicate the observed vertical CO_2 differences (center) from Fig. 2 and uncertainties (width) (*25*). The lines in each plot are linear least-squares fits to the modeled values.

References and Notes

1. A. S. Denning, I. Y. Fung, D. Randall, *Nature* **376**, 240 (1995).
2. P. P. Tans, I. Y. Fung, T. Takahashi, *Science* **247**, 1431 (1990).
3. P. Peylin, D. Baker, J. Sarmiento, P. Ciais, P. Bousquet, *J. Geophys. Res.* **107**, 4385 (2002).
4. K. R. Gurney *et al.*, *Nature* **415**, 626 (2002).
5. K. R. Gurney *et al.*, *Global Biogeochem. Cycles* **18**, GB1010 (2004).
6. P. Ciais, P. P. Tans, M. Trolier, J. W. C. White, R. J. Francey, *Science* **269**, 1098 (1995).
7. R. F. Keeling, S. C. Piper, M. Heimann, *Nature* **381**, 218 (1996).
8. P. Friedlingstein *et al.*, *Global Biogeochem. Cycles* **9**, 541 (1995).
9. R. B. Myneni, C. D. Keeling, C. J. Tucker, G. Asrar, R. R. Nemani, *Nature* **386**, 698 (1997).
10. D. Schimel *et al.*, *Science* **287**, 2004 (2000).
11. S. W. Pacala *et al.*, *Science* **292**, 2316 (2001).
12. C. C. Barford *et al.*, *Science* **294**, 1688 (2001).
13. W. De Vries, G. J. Reinds, P. Gundersen, H. Sterba, *Glob. Change Biol.* **12**, 1151 (2006).
14. J. Grace *et al.*, *Science* **270**, 778 (1995).
15. O. L. Phillips *et al.*, *Science* **282**, 439 (1998).
16. R. S. DeFries *et al.*, *Proc. Natl. Acad. Sci. U.S.A.* **99**, 14256 (2002).
17. R. A. Houghton, *Tellus* **55B**, 378 (2003).
18. F. Achard, H. D. Eva, P. Mayaux, H. Stibig, A. Belward, *Global Biogeochem. Cycles* **18**, GB2008 (2004).
19. S. L. Lewis, *Philos. Trans. R. Soc. London Ser. B* **361**, 195 (2006).
20. C. Rödenbeck, S. Houweling, M. Gloor, M. Heimann, *Tellus* **55B**, 488 (2003).
21. A. Jacobson, S. Mikaloff Fletcher, N. Gruber, J. Sarmiento, M. Gloor, *Global Biogeochem. Cycles* **21**, GB1020 (2007).
22. M. Tanaka, T. Nakazawa, S. Aoki, *J. Geophys. Res.* **88**, 1339 (1983).
23. R. J. Francey, L. P. Steele, R. L. Langenfelds, B. C. Pak, *J. Atmos. Sci.* **56**, 279 (1999).
24. GLOBALVIEW-CO_2, Cooperative Atmospheric Data Integration Project—Carbon Dioxide, CD-ROM, NOAA GMD, Boulder, CO (2006); available online via anonymous FTP to ftp.cmdl.noaa.gov, path: ccg/co2/GLOBALVIEW.
25. Materials and methods are available as supporting material on *Science* Online.
26. A. S. Denning, T. Takahashi, P. Friedlingstein, *Tellus* **51B**, 249 (1999).

27. R. K. Dixon *et al.*, *Science* **263**, 185 (1994).
28. I. A. Janssens *et al.*, *Science* **300**, 1538 (2003).
29. J. Lloyd, G. D. Farquhar, *Funct. Ecol.* **10**, 4 (1996).
30. S. R. Saleska *et al.*, *Science* **302**, 1554 (2003).
31. K. W. Holmes *et al.*, *Global Biogeochem. Cycles* **20**, GB3004 (2006).
32. A. D. McGuire *et al.*, *Global Biogeochem. Cycles* **15**, 183 (2001).
33. D. F. Baker *et al.*, *Global Biogeochem. Cycles* **20**, GB1002 (2006).
34. We thank the following T3L2 modelers for sharing their model output with us: R. M. Law, P. J. Rayner, D. Baker, Y.-H. Chen, I. Y. Fung, S. Houweling, J. John, T. Maki, S. Maksyutov, P. Peylin, M. Prather, B. C. Pak, and S. Taguchi. We thank A. Jacobson for helpful discussions. This work was supported by funding from the NSF, which sponsors the National Center for Atmospheric Research. The Transcom 3 experiment was made possible through support from the NSF (OCE-9900310), the National Oceanic and Atmospheric Administration (NA67RJ0152, Amend 30), and the International Geosphere Biosphere Program/Global Analysis, Interpretation, and Modeling Project. The Zotino measurements are supported by the European Union through the TCOS-Siberia contract (EVK2-CT-2001-00131) within the Fifth Framework Program. The Bass Strait/Cape Grim aircraft sampling program was supported by the Australian Bureau of Meteorology (1992–98), and the CSIRO Office of Space Science and Applications (1999–2000).

Supporting Online Material

www.sciencemag.org/cgi/content/full/316/5832/1732/DC1
Materials and Methods
SOM Text
Figs. S1 to S9
Tables S1 to S5
References

31 October 2006; accepted 9 May 2007
10.1126/science.1137004

Saturation of the Southern Ocean CO_2 Sink Due to Recent Climate Change

Corinne Le Quéré,[1,2,3]* Christian Rödenbeck,[1] Erik T. Buitenhuis,[1,2] Thomas J. Conway,[4] Ray Langenfelds,[5] Antony Gomez,[6] Casper Labuschagne,[7] Michel Ramonet,[8] Takakiyo Nakazawa,[9] Nicolas Metzl,[10] Nathan Gillett,[11] Martin Heimann[1]

Based on observed atmospheric carbon dioxide (CO_2) concentration and an inverse method, we estimate that the Southern Ocean sink of CO_2 has weakened between 1981 and 2004 by 0.08 petagrams of carbon per year per decade relative to the trend expected from the large increase in atmospheric CO_2. We attribute this weakening to the observed increase in Southern Ocean winds resulting from human activities, which is projected to continue in the future. Consequences include a reduction of the efficiency of the Southern Ocean sink of CO_2 in the short term (about 25 years) and possibly a higher level of stabilization of atmospheric CO_2 on a multicentury time scale.

Atmospheric CO_2 increases at only half the rate of human-induced CO_2 emissions because of the presence of large CO_2 sinks in the ocean and on land (*1*). The sinks are highly variable and sensitive to climate, yet they are poorly constrained by observations. In the ocean, only the large-scale variability and trends in the equatorial and North Pacific have been quantified (*2*, *3*). In other regions, time-series observations and repeated survey analysis exist, but their extrapolation at the scale of a basin is problematic because of the presence of large regional variability (*4*–*6*). Data are particularly sparse in the Southern Ocean, where the magnitude of the CO_2 sink is heavily disputed (*7*, *8*), its interannual variability is unknown, and its control on atmospheric CO_2 during glaciations is firmly established but still not understood or quantified (*9*, *10*).

We estimated the variability and trend in the CO_2 sink of the Southern Ocean during 1981 to 2004 using the spatiotemporal evolution of atmospheric CO_2 from up to 11 stations in the Southern Ocean and 40 stations worldwide (Fig. 1). We used an inverse method that estimates the CO_2 flux distribution and time variability that best matches the observed atmospheric CO_2 concentrations (*11*). The inversion uses observed atmospheric CO_2 concentrations from individual flask pair values and/or hourly values from in situ analyzers, as available (*12*) (fig. S1). The station set is kept constant throughout the inversion to minimize spurious variability from the inversion setup. We performed an identical inversion over four time periods using (i) 40 atmospheric stations for 1996 to 2004 (9 years), (ii) 25 atmospheric stations for 1991 to 2004 (14 years), (iii) 17 atmospheric stations for 1986 to 2004 time period (19 years), and (iv) 11 atmospheric stations for 1981 to 2004 (24 years). CO_2 fluxes and concentrations are linked by the atmospheric transport model TM3, with resolution of ~4° by 5° and 19 vertical levels, driven by interannual 6-hourly winds from National Centers for Environmental Prediction (NCEP) reanalysis (*13*). The a priori information does not involve any time-dependent elements. Although we focus on the Southern Ocean (south of 45°S), where the influence of the land is at its minimum, the inversion is global.

The variability in integrated sea-air CO_2 flux estimated by the inversions is ±0.14 Pg C year^{-1} (*14*) over the Southern ocean (Fig. 2). The

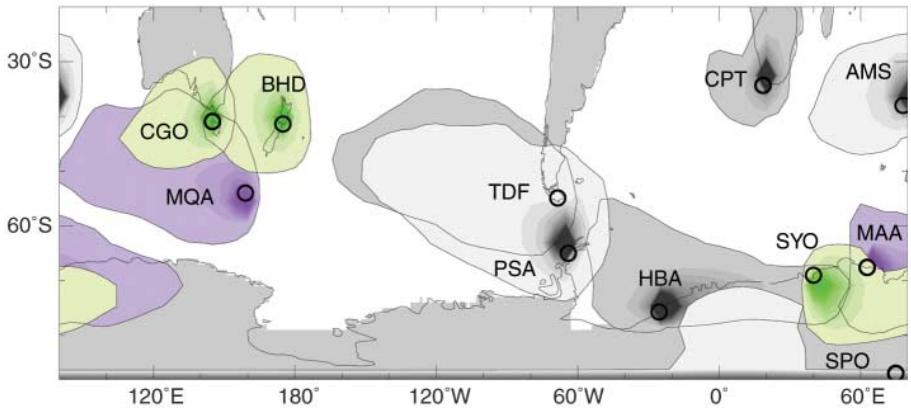

Fig. 1. Footprint of atmospheric CO_2 measurement stations. The footprint is defined here as the area where CO_2 fluxes of 0.2 mol/m^2 year^{-1} produce a concentration response of at least 1 ppm, on an annual average. The darkest shading shows the region with largest influence on a given station. Stations are Cape Grim (CGO; 40.7°S, 144.7°E); Macquarie Island (MQA; 54°S, 159°E); Baring Head (BHD; 41°S, 175°E); Tierra del Fuego (TDF; 54.9°S, 68.5°W); Palmer Station (PSA; 65.0°S, 64°W); Halley Bay (HBA; 75.7°S, 25.5°W); Cape Point (CPT; 34°S, 19°E); Syowa (SYO; 69°S, 39°E); Mawson (MAA; 68°S, 63°E); Amsterdam Island (AMS; 38°S, 78°E); and South Pole (SPO; 90.0°S). The color coding refers to the length of the station's record used, with light gray stations used since 1981, green stations since 1986, purple stations since 1991, and dark gray stations since 1996.

[1]Max Planck Institut für Biogeochemie, Postfach 100164, D-07701 Jena, Germany. [2]School of Environmental Sciences University of East Anglia, Norwich NR4 7TJ, UK. [3]British Antarctic Survey, High Cross, Madingley Road, Cambridge CB3 0ET, UK. [4]National Oceanic and Atmospheric Administration, Earth System Research Laboratory, 325 Broadway, Boulder, CO 80305, USA. [5]Commonwealth Scientific and Industrial Research Organisation, Marine and Atmospheric Research, PMB1 Aspendale, Victoria 3195, Australia. [6]National Institute for Water and Atmospheric Research, P.O. Box 14901, Wellington, New Zealand. [7]South African Weather Service, P.O. Box 320, Stellenbosch, 7599 South Africa. [8]Laboratoire des Sciences du Climat et de l'Environnement/Institut Pierre Simon Laplace (LSCE/IPSL), Gif-sur-Yvettes, Cedex 91191, France. [9]Center for Atmospheric and Oceanic Studies, Tohoku University, Sendai 980-8578, Japan. [10]Laboratoire d'Océanographie et du Climat: Experimentation et Approaches Numériques (LOCEAN/IPSL) CNRS, Université Pierre and Marie Curie, Paris, France. [11]Climate Research Unit, School of Environmental Sciences, University of East Anglia, Norwich NR4 7TJ, UK.

*To whom correspondence should be addressed. E-mail: c.lequere@uea.ac.uk